

# Effect of milling time on electrochemical properties of $\text{CaNi}_{4.8}\text{Mg}_{0.2}$ anode material of Ni-MH battery

Imen Karaoud<sup>1</sup>, Youssef Dabaki<sup>1,2</sup>, Yassine Ben Belgacem<sup>1</sup>, Chokri Khaldi<sup>1</sup>, Omar ElKedim<sup>3</sup>, Nouredine Fenineche<sup>4</sup>, Jilani Lamloumi<sup>1</sup>

<sup>1</sup> Université de Tunis, ENSIT, LR99ES05, 1008 Montfleury, Tunisia

<sup>2</sup> Laboratoire de Physico-Chimie de l'Atmosphère (LPCA), Université du Littoral Côte d'Opale (ULCO), EA 4493, 59140 Dunkerque, France

<sup>3</sup> FEMTO-ST, MN2S, UTBM, UBFC, 90010 Belfort Cedex, France.

<sup>4</sup> ICB-PMDM/FR FCLAB, UTBM, UBFC, 90010 Belfort Cedex, France

Correspondence

Youssef Dabaki, Université de Tunis, ENSIT, LR99ES05, 1008 Montfleury, Tunisia

Email: [dabakiyoussef@gmail.com](mailto:dabakiyoussef@gmail.com)

**Abstract** Recently, due to the rapid advances in hydrogen storage research and Ni-MH rechargeable batteries, great attention has been given to the development of more efficient hydride alloys used in negative electrodes. Among these hydrogen storage materials, metal hydrides of type  $\text{AB}_5$ , particularly  $\text{LaNi}_5$ , are the most extensively studied in previous research works. However,  $\text{CaNi}_5$  alloy is a good alternative because of its low cost, great availability, excellent kinetic properties and high hydrogen storage capacity. This study focuses on  $\text{CaNi}_{4.8}\text{Mg}_{0.2}$  alloy used as the negative electrode of Ni-MH batteries. In the performed experiments,  $\text{CaNi}_{4.8}\text{Mg}_{0.2}$  were synthesized through mechanical alloying using a Retsch PM400 ball mill for different milling times of 30, 40, 50 and 60 hours with a ball/powder weight ratio of 8:1 and under an argon atmosphere. The main objective of the current research work is to investigate the effect of milling time on the structural, morphological and electrochemical properties of the  $\text{CaNi}_{4.8}\text{Mg}_{0.2}$  alloy. Electrochemical properties are examined employing various methods, such as galvanostatic and potentiodynamic polarization, at room temperature and in a KOH 6M electrolyte. The obtained results demonstrate that  $\text{CaNi}_{4.8}\text{Mg}_{0.2}$  alloy, with a milling time of 30 hours, exhibited the highest discharge capacity, the greatest reversibility and the best kinetics, compared to the alloys milled for 40, 50 and 60 hours.

**Keywords**  $\text{CaNi}_{4.8}\text{Mg}_{0.2}$  type alloy, Mechanical alloying, Ni-MH Battery, Electrochemical polarization technique

## 1 Introduction

The manufacturing and use of the electronic devices, including laptops, electric vehicles and cell phones, have increased dramatically in the last decades (Ref 1,2). Moreover, the escalating air pollution levels and stricter emission standards imposed on combustion vehicles have led to a growing interest in electric and hybrid vehicles (Ref 3,4). Though various modern batteries, such as lead-acid battery, Ni-Cd battery and Li-ion battery, were developed (Ref 5-9), none of them are efficient, cost-effective, safe and eco-friendly (Ref 10). To meet these new demands, Ni-MH batteries were produced and became the most commonly used thanks to their excellent discharge capacity, long lifespan and eco-friendly properties (Ref 11-13). They have been developed and marketed, since the 1990s (Ref 14,15), and have become a key component of advanced information and telecommunications systems as well as the next generation of hybrid or fully-electric vehicles (Ref 16,17). In fact, their performance depends not only on that of the active materials in the negative electrode (Ref 18), but also on the procedure of producing the latter (Ref 19). In this context, several manufacturing methods were introduced in the literature and used in many studies (Ref 20-22). For instance, mechanical alloying is commonly employed to synthesize metal hydrides (Ref 23-25). This simple and cost-effective technique offers numerous advantages including easy and controlled synthesis (Ref 26). Moreover, metal hydrides have been utilized in rechargeable batteries for hydrogen storage (Ref 27, 28). In such batteries, the hydrogen atoms are stored, by the following compound types  $AB_5$  (Ref 29, 30),  $AB_3$  (Ref 31, 32),  $AB_2$  (Ref 33, 34),  $AB$  (Ref 35, 36) and  $A_2B_7$  (Ref 37, 38) in the solid material at interstitial positions (Ref 39). In fact, the  $AB_5$  type is the most widely popular and extensively studied compound. It crystallizes in the hexagonal structure of the  $CaCu_5$  type in the space group  $P6/mmm$  (Ref 40, 41, 42). It has storage capacity of about 1.5 wt%, using the solid-gas method (Ref 43), and electrochemical discharge capacity of  $370 \text{ mAhg}^{-1}$  (Ref 44, 45). The  $AB_5$  type alloy is known by its capability

to easily substitute compounds A and B with other elements (Ref 46). In fact, A is usually lanthanum that may be partially or entirely substituted with Yttrium (Y) (Ref 47), Calcium (Ca) (Ref 48), Mischmetal (Mm) (Ref 49), Cerium (Ce) (Ref 50) or Zirconium (Zr) (Ref 51). However, B is frequently nickel which can be substituted with several transition elements (Ref 52) such as Aluminum (Al) (Ref 53), Manganese (Mn) (Ref 54), Zinc (Zn) (Ref 55), Tin (Sn) (Ref 56), Fer (Fe) (Ref 57) and Cobalt (Co) (Ref 58). A. Merzouki et al. (Ref 59) carried out a comparative study of the compounds  $\text{LaNi}_{3.55}\text{Mn}_{0.4}\text{Al}_{0.3}\text{Co}_{0.75}$ ,  $\text{LaNi}_5$ , and its mono-substituted derivatives. From the obtained findings, the authors proved that the tri-substituted compound exhibited the highest stability and longest lifetime, compared to the three other compounds. Due to the considerably high cost of lanthanum (La), it can be completely replaced by calcium (Ca). In addition, the  $\text{CaNi}_5$  compound possesses a theoretical discharge capacity of  $482 \text{ mAhg}^{-1}$  surpassing that of  $\text{LaNi}_5$  ( $372 \text{ mAhg}^{-1}$ ). Therefore, it is possible to enhance the performance of the metal hydride  $\text{LaNi}_5$  by replacing lanthanum with calcium (Ref 60). The  $\text{CaNi}_5$  compound is also characterized by its high electrochemical discharge capacity albeit and limited cyclic stability (Ref 61). Attempts have, therefore, been made to improve the hydrogen storage properties of  $\text{CaNi}_5$  by partially substituting Ca and/or Ni with other elements. For example, J.O. Jensen et al. (Ref 62) investigated the impact of substituting Ni, in the basic  $\text{CaNi}_5$ -compound, with various metals (Al, Cr, Mn, Co, Fe, Cu, Zn, Sn and Mg) at two substitution rates  $x=0.5$  and 1. Their findings reveal that all the electrodes were easily activated. It was also observed that only the  $\text{CaNi}_{5-x}\text{M}_x$  ( $M= \text{Cu, Zn, and Mg}$ ) electrodes preserved the same discharge capacity as  $\text{CaNi}_5$ . The  $\text{CaNi}_{5-x}\text{M}_x$  ( $M= \text{Zn and Mg}$ ) electrodes showed superior electro-chemical discharge capacity of  $100 \text{ mAhg}^{-1}$  and enhanced stability, compared to  $\text{CaNi}_5$ . Besides, partial substitution of the nickel allows for maintaining its main characteristics such as high electro-chemical discharge capacity, outstanding cyclic stability, rapid atomic hydrogen diffusion within the lattice and long lifetime (Ref 63). G.liang

et al. (Ref 64) explored the influence of partial substitution of  $\text{CaNi}_5$  by Mn, Zn, and Al on the electro-chemical properties. They demonstrated that the combination of the substitution of Ca with Mn and that of Ni with Zn and Al significantly strengthen electrode stability. Nevertheless, it was proven that the substitution of Zn and Al does not necessarily prevent the degradation of the electrode and the reduction of its electrochemical discharge capacity. S. Chumphongphan et al. (Ref 65) compared the hydrogen storage properties of  $\text{CaNi}_{5-x}\text{M}_x$  (M=Mo, Al) compounds for  $x= 0.1$  and  $0.2$  with that of the  $\text{CaNi}_5$  compound. Indeed, all the used electrodes had higher maximum discharge capacities than  $\text{CaNi}_5$  and only the cycling stability of the  $\text{CaNi}_{4.9}\text{Al}_{0.1}$  electrode was improved. Y. Dabaki et al. (Ref 66,67) studied the  $\text{CaNi}_{5-x}\text{Mn}_x$  ( $x=0.3, 0.5, 1$ ) compound elaborated by mechanical alloying at different milling times (2, 10, 20, 30, 40, 50 and 60h). The electro-chemical results indicated that, for the three substitutions  $x=0.3, 0.5, 1$ , the maximum discharge capacities, which were respectively equal to 125, 119 and 109  $\text{mAhg}^{-1}$ , were obtained at a milling time of 40h.

Within the same framework, the current work is an extension of a previous study (Ref 68) focusing on the  $\text{CaNi}_{4.8}\text{Mg}_{0.2}$  compounds prepared for 40h of mechanical milling and 8:1 ball-to-powder weight ratio. It analyzes the structural, morphological and electro-chemical properties of  $\text{CaNi}_{4.8}\text{Mg}_{0.2}$  compounds at different milling times 30, 40, 50 and 60 h.

## 2. Experimental

### 2.1 Synthesis and characterization of $\text{CaNi}_{4.8}\text{Mg}_{0.2}$ (30, 40, 50 and 60 h) powders

Mechanical alloying is a technique applied to process homogeneous powdered materials through the fracturing of particles by shock. It is also used to produce powders with sizes up to tens of nanometers, simultaneously creating supplementary active sites to enhance hydrogen penetration (Ref 69). In the conducted experiments,  $\text{CaNi}_{4.8}\text{Mg}_{0.2}$  powders were obtained by the mechanical alloying method using a Retsch PM400 high-energy planetary ball mill with 400 rpm angular speed at different milling times (30, 40, 50 and 60h) and at a ball-to-powder weight ratio of 8:1 in an argon atmosphere and at room temperature. After the

synthesis of the powders, structural and morphological characterization was performed using, respectively, Bruker D8 Advance XRD with  $\text{CoK}\alpha$  radiation ( $\lambda = 1.789 \text{ \AA}$ ) and scanning electron microscope SEM JEOL JSM -5800LV.

## **2.2 Electro-chemical characterization of $\text{CaNi}_{4.8}\text{Mg}_{0.2}$ (30, 40, 50, 60h) electrodes**

### **2.2.1 Preparation of the working electrode and the electro-chemical cell**

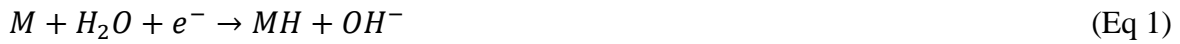
The electro-chemical characterization of the  $\text{CaNi}_{4.8}\text{Mg}_{0.2}$  (30, 40, 50, 60 h) negative electrodes was carried out employing the electro-chemical device Galvanostat-Potentiostat Ec-Lab system (Biologic<sup>TM</sup>). The utilized electro-chemical cell was connected to the device through its three electrodes: a working electrode (negative electrode), an auxiliary electrode (positive electrode), formed by a coiled nickel wire to increase its surface, and a reference electrode (Hg/HgO) replete with potassium and employed to assess its equilibrium potential. All the electrodes were immersed in a 6M KOH electrolyte. Then, the metal hydride electrode (working electrode) was prepared utilizing the so-called 'Latex' technique (Ref 70,71). Firstly, 90% of the alloy powder was mixed with 5% of black carbon in order to increase the electronic conductivity of the electrode. It was noticed that 5% of fine particles of polytetrafluoroethylene (PTFE) acted as a mechanical binder to make the electrode elastic. Afterwards, the whole mixture was wetted with ethanol and agitated until obtaining a paste. The latter was spread with a glass roller several times until the ethanol evaporated and a paste was formed (latex) (Ref 72). Finally, once the paste dried under vacuum for 24 hours at room temperature, the formed "Latex" was into pieces. Subsequently, the latter were compressed on both sides of the nickel grid acting as a current collector, to  $0.5 \text{ cm}^2$ , to form the working electrodes. The wire ensuring the electrical contact between latex and the circuit was made of nickel.

## 2.2.2 The different electro-chemical characterization techniques

Galvanostatic polarization entails the application of a constant current between the working electrode and the auxiliary one during the charge/discharge cycles to measure the potential between the working and the reference electrodes as a function of time.

The true charge capacity was not experimentally accessible because the cell was open, which made it impossible to determine the amount of monoatomic hydrogen inserted into the negative electrode, which is competitive with the quantity of the released hydrogen gas.

- Charge reaction:



- Hydrogen release:



During discharge, no outgassing was observed and the electrochemical discharge capacity was measured according to the discharge reaction written below:



By using the chronopotentiogram, the discharge capacity of the negative electrode at each cycle was determined applying the following equation:

$$C_{th}(mAh/g) = i(mA) \cdot \frac{t(h)}{m(g)} \quad (\text{Eq 4})$$

m: Mass of the alloy in the negative electrode (g),

i: Discharge current (mA),

t: Discharge time (h).

Potential-dynamic polarisation involves applying a potential  $E_{app}$  ranging from -0.6 to -1.3 V, on the working electrode and vice versa, and varying linearly with time at a slow rate  $v=1mVs^{-1}$ , according to the following equation:

$$E_{app} = \pm vt + E_i \quad (\text{Eq 5})$$

The obtained voltammogram was based on the theoretical Butler-Volmer equation expressed as a function of the anode and cathode current:

$$I = I_0 [\exp(b_a(E_{app} - E_0)) - \exp(b_c(E_{app} - E_0))] \quad (\text{Eq 6})$$

where  $b_a$  and  $b_c$  are the anodic and cathodic Tafel constants, respectively;  $E_0$  is the Nernst potential (V) and  $I_0$  denotes the exchange current density ( $\text{A g}^{-1}$ ). These parameters were determined by applying Stern's first rule on the voltammograms,  $I=f(E_{app})$ , to provide the Tafel curve,  $\log I=f(E_{app})$

### 3. Result and discussion

#### 3.1 Structural and morphological characterization of $\text{CaNi}_{4.8}\text{Mg}_{0.2}$ (30, 40, 50 and 60 h) powders

##### 3.1.1 Structural characterization

Figure 1 shows the XRD patterns of the  $\text{CaNi}_{4.8}\text{Mg}_{0.2}$  powder at different milling times (30, 40, 50 and 60 h).

These patterns were refined utilizing X'Pert High Score software. This refinement allowed identifying the existing phases of  $\text{CaNi}_{4.8}\text{Mg}_{0.2}$  powders and determining the lattice parameters and the average crystallite size which are presented in Table 1.

Table 1 shows the various crystallographic parameters of the  $\text{CaNi}_{4.8}\text{Mg}_{0.2}$  powders obtained at 30, 40, 50 and 60 h milling times.

For 30 h of milling (Fig. 1a), the XRD pattern reveals the presence of two main phases Ni (cubic) and  $\text{CaNi}_5$  (hexagonal) located, respectively, at the following positions  $51.99^\circ$ ,  $60.8^\circ$ ,  $91.40^\circ$  and  $24.74^\circ$ ,  $36.75^\circ$ ,  $42.92^\circ$ ,  $51.99^\circ$   $57.23^\circ$ . The presence of the  $\text{CaNi}_5$  phase was due to the dissolution of Ni atoms (atomic radius =  $1.4\text{\AA}$ ) in the Ca lattice (atomic radius =  $1.8\text{\AA}$ ) (Ref 73,74). Previous studies dealing with the effect of milling time on  $\text{CaNi}_5$ -based alloy demonstrated that the appearance of a strong halo peak between the  $30^\circ < 2\theta < 55^\circ$  position indicated the formation of an amorphous phase and the nanocrystalline nickel phase (Ref 75, 76). Additional investigations revealed that, within the timeframe ranging from 10 to 40h of

milling, a continuous decrease in peak intensity coupled with the broadening of its width was observed, suggesting a partial amorphization process (Ref 74,77).

The continuous milling during 40, 50 and 60h (Fig. 1b, c, d) showed similar phases of Ni and CaNi<sub>5</sub>. A progressive shift of the principal diffraction peaks towards the highest angular positions 51.74°, 51.85°, 52.02° and 52.08°, respectively, as well as an increase in intensities and a reduction in peak broadening were observed at 30, 40, 50 and 60h milling times. During the milling process, a temperature increase, attributed to the contact between the balls and the powder and leading to the inversion of energy kinetic in the balls into heat, was also noticed. Moreover, the prolonged milling time resulted in a progressive temperature rise, promoting the emergence of a crystalline phase (Ref 78,79). Therefore, the partial amorphization process was followed by crystallization.

Using Scherrer method, it was found that, as the milling time increased from 30h to 60 h, the average crystallite size of Ni and CaNi<sub>5</sub> decreased gradually from 11.8 to 4.1 nm and from 7.5 to 3.2 nm, respectively.

### **3.1.2 Morphological characterization**

Figure 2 exposes the morphology of CaNi<sub>4.8</sub>Mg<sub>0.2</sub> (30, 40, 50 and 60 h) powders.

SEM observation is used to visualize the size and distribution of the powder particles. During 30 h milling time, the micrograph of the powder reveals the existence of agglomerates with an average particle size of 27 μm. By increasing the milling time to 40 h, the average particle size decreases to almost 22 μm, indicating that the milling process achieved a fracturing stage on the agglomerated powder to form fine particles. The longer the milling time was, the more homogeneous the morphology. During 50 and 60 h milling times, the particle size is respectively equal to 22 and 20 μm and the agglomerates gradually take on a rounded shape. Moreover, the particle size remains remarkably consistent and



relatively stable due to the achievement of a certain equilibrium state during this milling stage.

Figure 3 shows the histogram of the average particle size distribution of  $\text{CaNi}_{4.8}\text{Mg}_{0.2}$  (30, 40, 50 and 60 h) powders.

In this histogram, the bars represent the number of particles classified according to the average particle size. It contains into 7 classes. The most frequent size class, of all powder, is between 0 and  $20\mu\text{m}$ . However, the second class, includes between 25 and 15 particles whose size ranges between 20 and  $40\mu\text{m}$ . Obviously, the number of particles continues to decrease in the other size classes until it reaches the last size class, which is the least frequent and contains only one particle with a size of  $220\mu\text{m}$ .

Figure 4 shows the EDX pattern of  $\text{CaNi}_{4.8}\text{Mg}_{0.2}$  (30, 40, 50 and 60 h) powders.

This quantification enabled the identification of the elements present in  $\text{CaNi}_{4.8}\text{Mg}_{0.2}$  powders. It can be deduced that the chemical composition of all elements of Ca, Ni and Mg powders is almost similar to the nominal composition of  $\text{CaNi}_{4.8}\text{Mg}_{0.2}$  (30, 40, 50 and 60 h) powders (Table 2).

### **3.2 Electro-chemical characterization of $\text{CaNi}_{4.8}\text{Mg}_{0.2}$ (30, 40, 50, and 60h) electrodes**

#### **3.2.1 Activation, cycling performance and polarization**

Figure 5 shows the evolution of the discharge potential as function of the electro-chemical discharge capacity of  $\text{CaNi}_{4.8}\text{Mg}_{0.2}$  electrode at different milling times (30, 40, 50 and 60h).

In the electro-chemical cycling, the metal compound was activated when its discharge capacity reached its maximum value, its half-discharge potential remained constant and its polarization became minimal (Ref 80).

During the repetitive charge-discharge cycles, the negative electrode will be activated, i.e., it will be fragmented and cracked thus increasing the active surface that facilitates the

absorption and desorption of hydrogen. The electrode surface was rapidly activated, which showed its efficiency in hydrogen absorption/desorption reactions (Ref 81).

The  $\text{CaNi}_{4.8}\text{Mg}_{0.2}$  (30h) electrode was activated during the 3<sup>rd</sup> cycle. However, the  $\text{CaNi}_{4.8}\text{Mg}_{0.2}$  electrode milled during 40, 50 and 60h, required only one cycle to be activated. Indeed, the obtained maximum discharge capacities were about  $118 \text{ mAhg}^{-1}$  (3<sup>rd</sup> cycle),  $87 \text{ mAhg}^{-1}$  (1<sup>st</sup> cycle),  $84 \text{ mAhg}^{-1}$  (1<sup>st</sup> cycle) and  $53 \text{ mAhg}^{-1}$  (1<sup>st</sup> cycle) at 30, 40, 50 and 60 h milling times, respectively.

Figure 6 represents the evolution of the electro-chemical discharge capacity as a function of the number of the charge/discharge cycles at different milling times. It was noticed that, after activation, the maximum discharge capacity decreased progressively with the increase of number of cycles due to the degradation of the active material. This decline led to the reduction of the interstitial sites of hydrogen insertion (Ref 82).

Table 3 summarizes the electrochemical cycling results, including the maximum discharge capacity ( $C_{\text{max}}$ ), the capacity at the 50<sup>th</sup> cycle ( $C_{50}$ ) and the loss of capacity ( $S_{50}(\%)$ ). The loss of capacity is determined according to the following equation:

$$S_{50}(\%) = \left( \frac{C_{\text{max}} - C_{50}}{C_{\text{max}}} \right) * 100 \quad (\text{Eq 7})$$

It reveals that the variation of the maximum discharge capacity has the same tendency as the stability cycles (i.e., they both decrease with the increase of the milling time). In other words, the rise of the milling time from 30 to 60 hours increased the active surface area of the compounds. It became more exposed to the aggressive 6M KOH electrolyte, which accelerated its oxidation and led, subsequently, to the formation of an oxide layer (Ref 83).

The reversibility of the charging and the discharging reaction of the  $\text{CaNi}_{4.8}\text{Mg}_{0.2}$  electrodes during 30, 40, 50, and 60 h deteriorated during cycling. Indeed, the polarization increased progressively from 40, 168, 274 and 246 mV at the first cycle of activation to 200, 259, 423 and 334 mV at the 50<sup>th</sup> cycle, respectively for 30 h, 40 h, 50 h and 60 h milling times (Fig. 7).

As a consequence, good reversibility reaction of the  $\text{CaNi}_{4.8}\text{Mg}_{0.2}$  electrode was obtained at 30h milling time which is in good agreement with its electro-chemical properties.

### 3.2.2 Kinetic parameters: current density and Nernst potential

Figure 8 shows the evolution of some typical experimental and theoretical Tafel curves during the cycling of  $\text{CaNi}_{4.8}\text{Mg}_{0.2}$  (30, 40, 50 and 60 h) electrodes. These curves were determined at a slow potential rate of  $1 \text{ mV s}^{-1}$ .

The kinetic properties of  $\text{CaNi}_{4.8}\text{Mg}_{0.2}$  (30, 40, 50, 60h) electrodes during long cycling were defined by the potentiodynamic method (Ref 84,85). They were studied by applying a linear potential of  $1\text{mVs}^{-1}$  on the negative electrode. Then, the voltammograms,  $I = f(E)$  was determined after every five charging and discharging cycles. Afterwards, the obtained voltammograms were processed by Ec-Lab software utilizing Stern's first method to plot the Tafel polarisation curves,  $\log|I| = f(E_{\text{app}})$ .

During the first activation cycles, the Tafel curves moved towards the positive potential where hydrogen insertion into the electrode became easier. In fact, the values of the potential of the  $\text{CaNi}_{4.8}\text{Mg}_{0.2}$  (30, 40, 50, 60 h) electrodes in the first cycle were about -921, -835, -842, -899 mV, respectively. However, in the 20<sup>th</sup> cycle, the potential values were almost equal to -915, -831, -812 and -762 mV, respectively for the  $\text{CaNi}_{4.8}\text{Mg}_{0.2}$  (30, 40, 50, 60 h) electrodes. After activation, the curves shifted towards less positive potential where the insertion of hydrogen into the electrode became more difficult. Indeed, the values of the potential of the  $\text{CaNi}_{4.8}\text{Mg}_{0.2}$  electrodes at the 25<sup>th</sup> cycle were about -918, -843, -813 and -795 mV. However, at the 50<sup>th</sup> cycle, they were almost equal to -921, -837, -831 and -767mV at 30, 40, 50 and 60 h milling times, respectively. This result could be explained by the phenomenon of the oxidation and dissolution of the active material of the electrode during the electro-chemical cycling. It can also result from the electrode ageing due to the aggressivity of the 6M KOH electrolyte exerted on the negative hydride electrode.

Figure 9 shows the evolution of Nernst potential as a function of number of cycles of  $\text{CaNi}_{4.8}\text{Mg}_{0.2}$  (30, 40, 50 and 60 h) electrodes.

It is obvious that, at 60 h milling time, the  $\text{CaNi}_{4.8}\text{Mg}_{0.2}$  electrode had a higher potential than the  $\text{CaNi}_{4.8}\text{Mg}_{0.2}$  (30, 40 and 50 h) electrodes which is about -780 mV, indicating that hydrogen insertion became easier, compared to the other milling times.

Figure 10 shows the evolution of the exchange current density during the cycling of the  $\text{CaNi}_{4.8}\text{Mg}_{0.2}$  electrodes at 30, 40, 50 and 60 h milling times.

It shows that the exchange current density, at the 30h milling time, attains its maximum value at the first activation cycles ( $1827 \text{ mA g}^{-1}$ ). Then, it gradually decreases progressively before stabilizing after the 40<sup>th</sup> cycle ( $50 \text{ mA g}^{-1}$ ). At the other milling times (40, 50 and 60h), the exchange current density represents the same pattern with a high value of about  $250 \text{ mA g}^{-1}$  at the 1<sup>st</sup> activation cycle before stabilizing at around the minimum values ( $\sim 10 \text{ mA g}^{-1}$ ).

### **3.3 Comparative study of the electro-chemical properties of $\text{CaNi}_{4.8}\text{Mg}_{0.2}$ and $\text{CaNi}_{4.8}\text{Mn}_{0.2}$ negative electrodes at different milling times**

Table 4 presents the different cycling parameters such as maximum discharge capacity, cycle stability and degradation rate of the  $\text{CaNi}_{4.8}\text{Mn}_{0.2}$  and  $\text{CaNi}_{4.8}\text{Mg}_{0.2}$  negative electrodes.

It demonstrates that the discharge capacity  $C_{\text{max}}$  reaches its maximum value at a milling time of 30 h ( $118 \text{ mA h g}^{-1}$ ) and 40 h ( $96 \text{ mA h g}^{-1}$ ), respectively, for  $\text{CaNi}_{4.8}\text{Mg}_{0.2}$  and  $\text{CaNi}_{4.8}\text{Mn}_{0.2}$  electrodes.

The substitution of Mn resulted in a slight enhancement of the cycling stability of  $\text{CaNi}_{4.8}\text{Mn}_{0.2}$  electrode and the largest loss of discharge capacity after the 50<sup>th</sup> cycle was observed at 50h and 60h milling times for both compounds  $\text{CaNi}_{4.8}\text{Mn}_{0.2}$  and  $\text{CaNi}_{4.8}\text{Mg}_{0.2}$ .

Özgen et al. (Ref 86) compared the effect of the substitution of different elements in the  $\text{CaNi}_5$  compound on its electrochemical properties (substitution of Ca by Sm, Y, Ti, Dy, Er

and Hf and Ni by the elements Mn, Mg, Sn, Al, Cu, Si, Zn, Cr, Fe and V). They found that the compound substituted with Mg had a discharge capacity slightly greater than that of the compound substituted with Mn, 36 and 35 mAhg<sup>-1</sup>, respectively. Furthermore, the authors also observed that the durability and stability of Mn were better than those of compared to Mg. Jenson et al. (Ref 87) examined the substitutions of Ni in CaNi<sub>5-x</sub>M<sub>x</sub> compound (Al, Cr, Mn, Fe, Co, Cu, Zn and Sn and Mg). Notably, the CaNi<sub>4.5</sub>Mg<sub>0.5</sub> compound exhibited higher discharge capacity, compared to CaNi<sub>4.5</sub>Mn<sub>0.5</sub>, with values of 390 and 195 mAhg<sup>-1</sup>, respectively. The cycles during which more than 50% of the maximum capacity was preserved are the 3<sup>rd</sup>, for CaNi<sub>4.5</sub>Mn<sub>0.5</sub>, and the 4<sup>th</sup> for CaNi<sub>4.5</sub>Mg<sub>0.5</sub>. This finding suggests that Mn substitution enhanced the cyclic stability of CaNi<sub>5</sub> electrode.

Table 5 shows the polarization of the potential on the activation of CaNi<sub>4.8</sub>Mg<sub>0.2</sub> and CaNi<sub>4.8</sub>Mn<sub>0.2</sub> electrodes.

It reveals that the polarization of CaNi<sub>4.8</sub>Mg<sub>0.2</sub> electrode reaches about 40 mV during the 30h milling time and, then, undergoes a remarkable increase to attain 168, 274 and 246 mV, respectively, for the 40, 50 and 60 h milling times. The CaNi<sub>4.8</sub>Mg<sub>0.2</sub> (30h) electrode has the best reversibility. On the other hand, the polarization CaNi<sub>4.8</sub>Mn<sub>0.2</sub> electrode milled during 30h is almost equal to 220 mV. Then, it decreases slowly to 212 mV, during 40h milling time. Finally, it rises to 218 and 325 mV during milling of 50 and 60h. It is clear that the highest reversibility of the charging and discharging reaction of the electrodes was obtained at 40h milling time.

Table 6 represents the kinetic parameters of the CaNi<sub>4.8</sub>Mn<sub>0.2</sub> and CaNi<sub>4.8</sub>Mg<sub>0.2</sub> electrodes determined at different milling times (30, 40, 50 and 60 h).

It reveals that the Specific exchange current density of CaNi<sub>4.8</sub>Mn<sub>0.2</sub> electrode, reaches its maximum value of 83 mA g<sup>-1</sup> at 40 h milling time. However, CaNi<sub>4.8</sub>Mg<sub>0.2</sub> electrode attains a maximum value at 30h milling time. Thus, good agreement between the maximum capacities

obtained for  $\text{CaNi}_{4.8}\text{Mn}_{0.2}$  (40h) and  $\text{CaNi}_{4.8}\text{Mg}_{0.2}$  (30h), and the maximum current densities observed for both electrodes can be observed.

#### **4. Conclusion**

In this paper, the structural, morphological and electro-chemical properties of  $\text{CaNi}_{4.8}\text{Mg}_{0.2}$  (30, 40, 50 and 60 h) electrodes milled during 30, 40, 50 and 60h were presented using XRD, SEM and electro-chemical methods (galvanostatic and potentiodynamic polarization). XRD patterns of  $\text{CaNi}_{4.8}\text{Mg}_{0.2}$  reveal the presence of two main phases Ni (cubic) and  $\text{CaNi}_5$  (hexagonal), and the crystallite size, determined by the Scherrer method, decreases with increasing of the milling time.

The electro-chemical study performed during activation and long cycling showed that:

- The  $\text{CaNi}_{4.8}\text{Mg}_{0.2}$  (30, 40, 50, 60 h) electrodes activated, respectively, during the 3<sup>rd</sup>, 4<sup>th</sup> and 1<sup>st</sup> cycles. Indeed, the obtained discharge capacity values were equal to 118, 87, 84 and 53  $\text{mAhg}^{-1}$ .
- After activation, the discharge capacity decreased progressively during cycling due to the degradation of the active material of the electrode.
- The  $\text{CaNi}_{4.8}\text{Mg}_{0.2}$  (30 h) electrode had better reversibility than the other electrodes. This result is in good agreement with its maximum discharge capacity and easy activation.
- The  $\text{CaNi}_{4.8}\text{Mg}_{0.2}$  electrode gave, at (30h), the maximum values of the kinetic parameters, which correlates well with its electro-chemical properties (i.e., rapid activation, maximum discharge capacity, etc.).

#### **References**

1. A. Ercetin, Application of the hot press method to produce new Mg alloys Characterization, mechanical properties, and effect of Al addition, *J. Mater. Eng. Perform*, 2021, **30**(6), p 4254–4262

2. L.B. Lave, C. T. Hendrickson and F. C McMichael, Environmental implications of electric cars, *Science*, 1995, 268, p 993–995
3. M. Menou, D. Ibrahim and R.A. Marc Review on use of phase change materials in battery thermal management for electric and hybrid electric vehicles., *Int. J. Energy Re.*, 2016, **40** (8), p 1011–1031
4. C. Tarhan and M.A. Çil, A study on hydrogen, the clean energy of the future: Hydrogen storage methods, *J. Eng. Storage*, 2021, **40**, p 102676
5. G.J. May, A. Davidson and B.Monahov, Lead batteries for utility energy storage: A review, *J. Eng. Storage*, 2018, **15**, p 145–157
6. E. Blumbergs, V. Serga, E. Platacis, M. Maiorov and A. Shishkin, Cadmium recovery from spent Ni-Cd batteries: a brief review, *Metals*, 2021, **11**, p 1714
7. G. Genchi, M. S. Sinicropi, G. Lauria, A. Carocci and A. Catalano, The effects of cadmium toxicity, *Int. J. Environ. Res. Public. Health*, 2020, **17**, p 3782
8. W. B. Hawley and J. Li, Electrode manufacturing for lithium-ion batteries—Analysis of current and next generation processing, *J. Energy Storage*, 2019, **25**, p 100862
9. C. Bibin, M. Vijayaram, V. Suriya, R.S. Ganesh and S. Soundarraj, A review on thermal issues in Li-ion battery and recent advancements in battery thermal management system, *Materials Today: Proceedings*, 2020, **33**, p 116–128
10. Y. Liu, H. Pan, M. Gao and Q. Wang, Advanced hydrogen storage alloys for Ni/MH rechargeable batteries, *J. Mater. Chem.*, 2011, **21**, p 4743–4755
11. Y. B. Belgacem, C. Khaldi, J. Lamloumi and H. Takenouti, Effect of the discharge rate on the electrochemical properties of LaY<sub>2</sub>Ni<sub>9</sub> hydrogen storage alloy, *J. Alloys Compd.*, 2015, **631**, p 7–14

12. M.A. Fetcenko, S.R. Ovshinsky, B. Reichman, K. Young, C. Fierro, J. Koch, A. Zallen, W. Mays, T. Ouchi, Recent advances in NiMH battery technology, *J. Pow. Sou.*, 2007, **165**, p 544–551
13. X. Chen, A. Chu, D. Li, Y. Yuan, X. Fan and Y. Deng, Development of the cycling life model of Ni-MH power batteries for hybrid electric vehicles based on real-world operating conditions, *J. Energy Storage*, 2021, **34**, p 101999
14. S. R. Ovshinsky and M. A. Fetcenko, Development of high catalytic activity disordered hydrogen-storage alloys for electrochemical application in nickel–metal hydride batteries, *Appl. Phys.*, 2001, **72**, p 239–244
15. J. Shin and J. W. Choi, Opportunities and reality of aqueous rechargeable batteries, *Adv. Energy Mater.*, 2020, **10**(28), p 2001386
16. K. V. Vidyanandan, Batteries for electric vehicles, *Power Manag. Inst.*, 2019, **20**, p 38
17. M. Tliha, C. Khaldi, S. Boussami, N. Fenineche, O. ElKedim, H. Mathlouthi and J. Lamloumi, Kinetic and thermodynamic studies of hydrogen storage alloys as negative electrode materials for Ni/MH batteries: a review, *J. Solid State Electrochem.*, 2014, **18**, p 577–593
18. G. H. Ağaoğlu and G. Orhan, Production and electrochemical characterization of MgNi alloys by molten salt electrolysis for Ni–MH batteries, *Int. J. Hydrog. Energy*, 2018, **43**, p 6266–6274
19. H. Inoue, T. Ueda, S. Nohara, N. Fujita and C. Iwakura, Effect of ball-milling on electrochemical and physicochemical characteristics of crystalline Mg<sub>2</sub>Ni alloy, *Electrochimica Acta*, 1995, **43**, p 2215–2219
20. D. G. Oliva, M. Fuentes, E. M. Borzone, G. O. Meyer and P. A. Aguirre, Hydrogen storage on LaNi<sub>5-x</sub>Sn<sub>x</sub>, Experimental and phenomenological Model-based analysis, *Energy Convers. Manag.*, 2018, **173**, p 113–122



21. R.N. ELSHAER and K.M. IBRAHIM, Study of Microstructure, Mechanical Properties, and Corrosion Behavior of As-Cast Ni-Ti and Ti-6Al-4V Alloys. *J. Mater. Eng. Perform.*, 2022, p 1–15
22. M. Balcerzak, Structural, Electrochemical and Hydrogen Sorption Studies of Nanocrystalline Ti-V-Co and Ti-V-Ni-Co Alloys Synthesized by Mechanical Alloying Method. *J. Mater. Eng. Perform.*, 2019, **28**(8), p 4838–4844
23. H. Aoyagi, K. Aoki and T. Masumoto, Effect of ball milling on hydrogen absorption properties of FeTi, Mg<sub>2</sub>Ni and LaNi<sub>5</sub>, *J. Alloys Compd.*, 1995, **231**, p 804–809
24. M. Pentimalli, F. Padella, L. Pilloni, E. Imperi and P. Matricardi, AB<sub>5</sub>/AB<sub>5</sub> composite material for hydrogen storage, *Int. J. Hydrogen Energy*, 2009, **34**, p 4592–4596
25. M.M Alam, P. Sharma, J. Huot, J. On the hydrogen storage properties of cast TiFe mechanically milled with an intermetallic LaNi<sub>5</sub> and rare-earth elements La and Ce. *Int. J. Hydrog. Energy*, 2023
26. P. G. Jamkhande, N. W. Ghule, A. H. Bamer and M. G. Kalaskar, Metal nanoparticles synthesis: An overview on methods of preparation, advantages and disadvantages, and application, *J. Drug Deliv. Sci. Technol.*, 2019, **5**, p 101174
27. J.B.v. Colbe, J.R.o Ares, J. Barale, M. Baricco, C. Buckley, G. Capurso, N. Gallandat, D.M. Grant, M.N. Guzik, I. Jacob, E.H. Jensen, T. Jensen, J. Jepsen, T. Klassen, M.V. Lototskyy, K. Manickam, A. Montone, Puszkiel, S. Sartori, D.A. Sheppard, A. Stuart, G. Walker, C.J. Webb, H. Yang, V. Yartys, A. Zuttel and M. Dornheim, Application of hydrides in hydrogen storage and compression: Achievements, outlook and perspectives, *Int. J. Hydrog. Energy*, 2019, **44**, p 7780–7808
28. A. El Kharbachi, E.M. Dematteis, K. Shinzato, S.C. Stevenson, L.J. Bannenberg, M. Heere and B.C. Hauback, Metal Hydrides and Related Materials, Energy Carriers for Novel Hydrogen and Electrochemical Storage, *J. Phys. Chem. C*, 2020, **124**, p 7599–7607

29. Y. Dabaki, C. Khaldi, O. ElKedim, N. Fenineche and J. Lamloumi, Phase structure and electrochemical characteristics of  $\text{CaNi}_{4.7}\text{Mn}_{0.3}$  hydrogen storage alloy by mechanical alloying, *J. Solid State Electrochem.*, 2022, **26**, p 457–468
30. W. Liao, W. Jiang, X.S. Yang, H. Wang, L. Ouyang and M. Zhu, Enhancing (de) hydrogenation kinetics properties of the  $\text{Mg}/\text{MgH}_2$  system by adding  $\text{ANi}_5$  (A = Ce, Nd, Pr, Sm, and Y) alloys via ball milling, *J. Rare Earths*, 2021, **39**, p 1010–1016
31. Y. Ben Belgacem, C. Khaldi and J. Lamloumi, The effect of the discharge rate on the electrochemical properties of  $\text{AB}_3$ -type hydrogen storage alloy as anode in nickel-metal hydride batteries, *Int. J. Hydrogen Energy*, 2017, **42**, p 12797–12807
32. M. Ayari, I. Sahli, M. Elghali, O. Ghodbane, H. Jaafar and M. Abdellaoui, Synthesis and characterizations of structural and electrochemical properties of  $\text{CeTi}_2\text{Ni}_{4.5}\text{Al}_{0.2}\text{Mn}_{0.3}\text{Cr}_4$   $\text{AB}_3$  type compound, *J. Alloys and Comp.*, 2021, **884**, p 161017
33. Y. Wu, Y. Peng, X. Jiang, H. Zeng, Z. Wang, J. Zheng and X. Li, Reversible hydrogenation of  $\text{AB}_2$ -type Zr–Mg–Ni–V based hydrogen storage alloys, *Progress in Natural Science: Mat. Int.*, 2021, **31**, p 319–323
34. W. LI-MIN, H. RI, Effects of Long-Term Aging on Properties and Laves Phase Evolution of A New Type of Fe-Based Superalloy, *J. Mater. Eng. Perform.*, 2022, p. 1–11
35. B. Hosni, N. Fenineche, O. ElKedim, C. Khaldi and J. Lamloumi, Structural and electrochemical properties of TiFe alloys synthesized by ball milling for hydrogen storage, *J. Solid State Electrochem.*, 2018, **22**, p 17–29
36. M. Marinelli and M. Santarelli, Hydrogen storage alloys for stationary applications, *J. Energy Storage*, 2020, **32**, p 101864
37. M. Nowak, M. Balcerzak and M. Jurczyk, Effect of Substitutional Elements on the Thermodynamic and Electrochemical Properties of Mechanically Alloyed  $\text{La}_{1.5}\text{Mg}_{0.5}\text{Ni}_{7-x}\text{M}_x$  alloys (M = Al, Mn), *Metals*, 2020, **10**, p 578

38. A. Deng, Y. Luo, J. Zhou, Y. Xie, Y. Yuan, X. Kang, H. Zhang, Effect of Mn Element on the Structures and Properties of  $A_2B_7$ -Type La–Y–Ni-Based Hydrogen Storage Alloys, *Metals*, 2022, **12**(7), p 1122
39. U. Eberle, G. Arnold and R. Von Helmolt, Hydrogen storage in metal–hydrogen systems and their derivatives, *J. Power Sources*, 2006, **154**, p 456–460
40. J.M. Joubert, M. Latroche and A.P. Guégan, Metallic Hydrides II: Materials for Electrochemical Storage, *MRS bulletin*, 2007, **27**, p 694–698
41. W.L. Mi, Z.S. Liu, T. Kimura, A. Kamegawa and H.L. Wang, Crystal structure and hydrogen storage properties of  $(La,Ce)Ni_{5-x}M_x$  ( $M = Al, Fe, \text{ or } Co$ ) alloys, *International Journal of Minerals, Metall. and Mat.*, 2019, **26**, p 1–108
42. X. Chen, J. Xu, W. Zhang, S. Zhu, N. Zhang, D. Ke, J. Liu, K. Yan and H. Cheng, Effect of Mn on the long-term cycling performance of  $AB_5$ -type hydrogen storage alloy, *Int. J. Hydrogen Energy*, 2021, **46**, p 21973–21983
43. A. Singh, B.K. Singh, D.J. Davidson and O.N. Srivastava, Studies on improvement of hydrogen storage capacity of  $AB_5$  type:  $MmNi_{4.6}Fe_{0.4}$  alloy, *Int. J. Hydrogen Energy*, 2004, **29**, p 1151–1156
44. F. Liang, J. Lin, Y. Chng, D. Yin, Y. Wu and L. Wang, Gaseous sorption and electrochemical properties of rare-earth hydrogen storage alloys and their representative applications: A review of recent progress, *Sci. China Technol. Sci.*, 2018, **61**, p 1309–1318
45. Y. Liu, H. Pan, M. Gao and Q. Wang, Advanced hydrogen storage alloys for Ni/MH rechargeable batteries, *J. Mat. Chem.*, 2011, **21**, p 4743–4755
46. J. Xu, X. Chen, W. Zhu, W. Zhang, H. Cui, S. Zhu and H. Cheng, Enhanced cycling stability and reduced hysteresis of  $AB_5$ -type hydrogen storage alloys by partial substitution of Sn for Ni, *Int. J. Hydrogen Energy*, 2022, **47**(53), p 22495–22509

47. H. Zhang and L. Fu, Phase transformation relevant to the hydrogenation properties in the  $\text{YNi}_{3-x}\text{Cr}_x$ , *Chem. Phys. Lett.*, 2019, **736**, p 136823
48. M.L. Wasz. and R.B. Schwarz. Structure and properties of metal hydrides prepared by mechanical alloying. *Mater. Sci. Forum*, 1996, p 859–868
49. St. Todorova, V. Rangelova, L. Mihaylov and T. Spassov, Effect of hydrogen induced decrepitation on the hydrogen sorption properties of  $\text{MmNi}_5$ . *Int. J. Electrochem. Sci.*, 2020, **15**, p 4900 – 4907
50. J. Czub, W. Jamka, J. Przewoznik, A. Zarzecka, A. Hoser, D. Wallacher, N. Grimm and L. Gondek, Structural peculiarities in the b phase of the  $\text{La}_{0.75}\text{Ce}_{0.25}\text{Ni}_{4.8}\text{Al}_{0.2}$  Deuterides, *J. Alloys and Compounds*, 2019, **788**, p 533–540
51. E. Msika, M. Latroche, F. Cuevas and A.P. Guégan, Zr-substitution in  $\text{LaNi}_5$ -type hydride compound by room temperature ball milling, *Mater. Sci. Eng.*, 2004, **108**, p 91–95
52. Y. Chen, C.A. Sequeira, X. Song, R. Neto and Q. Wang, Polytypism of La–Ni phases in multicomponent  $\text{AB}_5$  type hydride electrode alloys, *Int. J. Hydrogen Energy*, 2002, **27**, p 63–68
53. M.H. Mendelsohn, D.M. Gruen and A.E. Dwight, The effect of aluminium additions on the structural and hydrogen absorption properties of  $\text{AB}_5$  Alloys with particular reference to the  $\text{LaNi}_{5-x}\text{Al}_x$  ternary alloy system, *J. The Less-Common Metals*, 1979, **63**, p 193 – 207
54. D.G. Westlake, A geometric model for the stoichiometry and interstitial site occupancy in hybrids (deutrides) of  $\text{LaNi}_5$ ,  $\text{LaNi}_4\text{Al}$  and  $\text{LaNi}_4\text{Mn}$ , *J. the Less-Common Metals*, 1938, **91**, p 275–292
55. M. Dymek, B. Rozdzyńska-Kielbik, V.V. Pavlyuk and H. Bala, Electrochemical hydrogenation properties of  $\text{LaNi}_{4.6}\text{Zn}_{0.4-x}\text{Sn}_x$  alloys, *J alloys and Comp.*, 2015, **644**, p 916–922

56. D.G. Olivaa, M. Fuentes, E.M. Borzoneb, G.O. Meyerb and P.A. Aguirrea, Hydrogen storage on  $\text{LaNi}_{5-x}\text{Sn}_x$ . Experimental and phenomenological Model-based analysis, *Eng. Conv. Manag.*, 2018, **173**, p 113–122
57. S.K. Pandey, A. Srivastava and O.N. Srivastava, Improvement in hydrogen storage capacity in  $\text{LaNi}_5$  through substitution of Ni by Fe, *Int. J. Hydrogen Energy*, 2007, **32**, p 2461– 2465
58. W.L. Mi, Z.S. Liu, T. Kimura, A. Kamegawa and H.L. Wang, Crystal structure and hydrogen storage properties of  $(\text{La,Ce})\text{Ni}_{5-x}\text{M}_x$  (M = Al, Fe, or Co) alloys, *International Int. J. Min. Metall. Mat.*, 2019, **26**, p 108–113
59. A. Merzouki, C. Cachet-Vivierb, V. Vivier, J.-Y. Nédélec, L.T. Yub, N. Haddaoui, J.-M. Joubert and A. Percheron-Guégan, Microelectrochemistry study of metal-hydride battery materials Cycling behavior of  $\text{LaNi}_{3.55}\text{Mn}_{0.4}\text{Al}_{0.3}\text{Co}_{0.75}$  compared with  $\text{LaNi}_5$  and its mono-substituted derivative, *J. Power Sources*, 2002, **109**, p 281–286
60. Z.P. Li and S. Suda, A new family of hydride electrode materials based on  $\text{CaNi}_5$ -type Alloys, *J. Alloys Compd*, 1995, **231**, p 751–754
61. P.D. Goodell, Stability of rechargeable hydriding alloys during extended cycling, *J. Less-Common Metals*, 1984, **99**, p 1–14
62. J.O. Jensen and N.J. Bjerrum, Systematic B-metal substitution in  $\text{CaNi}_5$ , *J. Alloys Compd.*, 1995, **293-295**, p 185–189
63. K. Hong, The development of hydrogen storage electrode alloys for nickel hydride batteries, *J. Power Sources*, 2001, **96**, p 85–89
64. G. Liang, S. Ruggeri, C. Lenain, H. Alamdari, J. Huot, L. Roue and R. Schulz, Synthesis of nanocrystalline  $\text{CaNi}_5$ -Based alloys and use for metal hydride electrode, *Mater. Sci. for*, 2001, **377**, p 71–76

65. S. Chumphongphan, M. Paskevicius, D.E. Sheppard and C.E. Buckley, Effect of Al and Mo substitution on the structural and hydrogen storage properties of  $\text{CaNi}_5$ . *Int. J. Hydrogen Energy*, 2013, **38**, p 2325–2331
66. Y. Dabaki, C. Khaldi, O. ElKedim, N. Fenineche and J. Lamloumi, Structural, morphological, and electrochemical properties of  $\text{AB}_5$  hydrogen storage alloy by mechanical alloying, *Env. Prog. Sust. Energy*, 2021, **41**, p 13739
67. Y. Dabaki, C. Khaldi, O. ElKedim, N. Fenineche and J. Lamloumi, Electrochemical properties of the  $\text{CaNi}_{5-x}\text{Mn}_x$  electrodes synthesized by mechanical alloying, *Int. J. Energy Research*, 2020, **44**, p 10112–10125
68. I. Karaoud, Y. Dabaki, C. Khaldi, O. ElKedim, N. Fenineche and J. Lamloumi, Electrochemical properties of the  $\text{CaNi}_{4.8}\text{M}_{0.2}$  ( $\text{M}=\text{Mg}$ ,  $\text{Zn}$ , and  $\text{Mn}$ ) mechanical milling alloys used as anode materials in nickel-metal hydride batteries, *Env. Prog. Sust. Energy*, 2023, p 14118
69. J.S. Benjamin, Mechanical Alloying. A Perspective, *Metal Powder Rep.*, 1990, **45**, p 122–127
70. M. Geng, J. Han, F. Feng and D.O. Northwood, Charging/discharging stability of a metal hydride battery electrode, *J. Electrochem. Soc.*, 1999, **146**, p 2371
71. W. Zayani, S. Azizi, M. Salah, K.S. El-Nasser, I. Othman Ali and J. Lamloumi, Structure and electrochemical hydrogen storage properties of spinel ferrites  $\text{Sm}_x\text{Zn}_{1-x}\text{Fe}_2\text{O}_4$  alloys ( $x = 0$ ,  $x = 0.2$ ,  $x = 0.4$ , and  $x = 0.6$ ) for Ni-MH accumulator applications, *Env. Prog. Sust. Energy*, 2022, p 14050
72. Y. Ben Belgacem, C. Khaldi, J. Lamloumi and H. Takenouti, The electrochemical performance of  $\text{AB}_3$ -type hydrogen storage alloy as anode material for the nickel metal hydride accumulators, *J. Solid State Electrochem.*, 2016, **20**, p 1949–1959

73. F. Popa, O. Isnard, I. Chicinaş, V. Pop, in *Proceedings of the 3rd International Conference on Powder Metallurgy*, 2005, 7–9
74. Y. Dabaki, C. Khaldi, N. Fenineche, O. ElKedim, M. Tliha, J. Lamloumi. Electrochemical studies on the Ca-based hydrogen storage alloy for different milling times, *Metals and Materials Int*, 2021, **27**, p1005–1024
75. G. Liang, J. Huot, R. Schulz. Mechanical alloying and hydrogen storage properties of CaNi<sub>5</sub>-based alloys, *J. of Alloys and Compounds*, 2001, **321**, p 146 –150
76. G. Liang, R. Schulz. Phase structures and hydrogen storage properties of Ca–Mg–Ni alloys prepared by mechanical alloying, *J. Alloys and Compounds*, 2003, **356–357**, p 612–616
77. B. Hosni, X. Li, C. Khaldi, O. ElKedim, J. Lamloumi. Structure and electrochemical hydrogen storage properties of Ti<sub>2</sub>Ni alloy synthesized by ball milling. *J. of Alloys and Compounds*, 2014, **615**, p 119–125
78. M.S. El-Eskandarany, *Mechanical Alloying, Nanotechnology, Materials Science and Powder Metallurgy*, 2<sup>nd</sup>, William Andrew, 2015
79. C. Suryanarayana, *Mechanical alloying and milling*, *Progress in Materials Science*, 2001, **46**, p 1–184
80. C. Khaldi, H. Mathlouthi and J. Lamloumi, A comparative study of 1M and 8M KOH electrolyte concentrations, used in Ni–MH batteries, *J. Alloys and Compd*, 2009, **469**, p 464–471
81. A. khedimallah, W. Zayani, Y. Dabaki, C. Khaldi, J. Lamloumi, O. El-Kedim and N. Fenineche, Electrochemical study of the LaNiO<sub>3</sub> perovskite-type oxide used as anode in nickel-metal hydride batteries, *Solid State Sciences*, 2023, **146**, 107338
82. W. Zayani, S. Azizi, K.S. El-Nasser, I. Othman Ali, M. Molière, N. Fenineche, H. Mathlouthi and J. Lamloumi, Electrochemical behavior of a spinel zinc ferrite alloy

- obtained by a simple sol-gel route for Ni-MH battery applications, *Int. J. Energy Research*, 2021, **45**, p 5235–5247
83. Y. Dabaki, S. Boussami, C. Khaldi, H. Takenouti, O. ElKedim, N. Fenineche and J. Lamloumi, The effect of ZnO addition on the electrochemical properties of the  $\text{LaNi}_{3.55}\text{Mn}_{0.4}\text{Al}_{0.3}\text{Co}_{0.2}\text{Fe}_{0.55}$  electrode used in nickel–metal hydride batteries, *J. Solid State Electroch.*, 2017, **21**, p 1157–1164
84. A. Khedimallah, Y. Dabaki, A. Kaabi, C. Khaldi, M. Molière, O. ElKedim, N. Fenineche, J. Lamloumi, Electrochemical study of the  $\text{LaFe}_{0.8}\text{Ni}_{0.2}\text{O}_3$  perovskite-type oxide used as anode in nickel-metal hydride batteries, *Ceram. Int.*, 2022, **48**, p 31157-31171
85. R. Dahsa, M. Dymek, Y. B. Belgacem, J. Lamloumi, C. Khaldi and H. Bala, Determination of  $\text{H}_2\text{O}/\text{H}_2$  system exchange current densities on cycled hydride electrodes from overswitch potential jump at low and high charge/discharge rates, *Int. J. Hydrogen Energy*, 2023, **48**, p 15203–15214
86. C. Özgen. Production and characterization of  $\text{CaNi}_{5-x}\text{M}_x$  compounds for metal hydride batterie. Middle East Technical University, 2012
87. J. O. Jensen, N. J. Bjerrum. Systematic B-metal substitution in  $\text{CaNi}_5$ . *J. Alloys Compd.*, 1999, **293**, p185–189.